ACS OMEGA

Article

Cite This: ACS Omega 2018, 3, 5799−5807

Facile Synthesis of Molybdenum Diselenide Layers for High-Performance Hydrogen Evolution Electrocatalysts

Dhanasekaran Vikraman,[†,‡] Sajjad Hussain,[§,∥] Kamran Akbar,[∥,○] Kathalingam Adaikalam,[#] Seung Hu Lee,[†] Seung-Hyun Chun,[⊥] Jongwan Jung,[§,∥] Hyun-Seok Kim,[‡] and Hui Joon Park*[,†,▽]

[†]Department of Energy Systems Research and [▽]Department of Electrical and Computer Engineering, Ajou University, 206 Worldcup-ro, Suwon 16499, Korea

[‡]Division of Electronics and Electrical Engineering and [#]Millimeter-wave Innovation Technology (MINT) Research Center, Dongguk University-Seoul, 30 Pildong-ro 1 gil, Jung-gu, Seoul 04620, Korea

[§]Institute of Nano and Advanced Materials Engineering, [∥]Graphene Research Institute, and [⊥]Department of Physics, Sejong University, 209 Neungdong-ro, Gwangjin-gu, Seoul 05006, Korea

[○]Department of Energy Science, Sungkyunkwan University, 2066 Seobu-ro, Jangan-gu, Suwon 16419, Korea

Supporting Information

ABSTRACT: A cost-effective solution-based synthesis route to grow $MoSe_2$ thin films with vertically aligned atomic layers, thereby maximally exposing the edge sites on the film surface as well as enhancing charge transport to the electrode, is demonstrated for hydrogen evolution reaction. The surface morphologies of thin films are investigated by scanning electron microscopy and atomic force microscopy, and transmission electron microscopy analyses confirm the formation of the vertically aligned layered structure of $MoSe_2$ in those films, with supporting evidences obtained by Raman. Additionally, their optical and compositional properties are investigated by photoluminescence and X-ray photoelectron spectroscopy, and their electrical properties are evaluated using bottom-gate field-effect transistors. The resultant pristine $MoSe_2$ thin film exhibited low overpotential of 88 mV (at 10 $mA{\cdot}cm^{-2}$) and a noticeably high exchange current density of 0.845 $mA{\cdot}cm^{-2}$ with excellent stability, which is superior to most of other reported MoS_2 or $MoSe_2$-based catalysts, even without any other strategies such as doping, phase transformation, and integration with other materials.

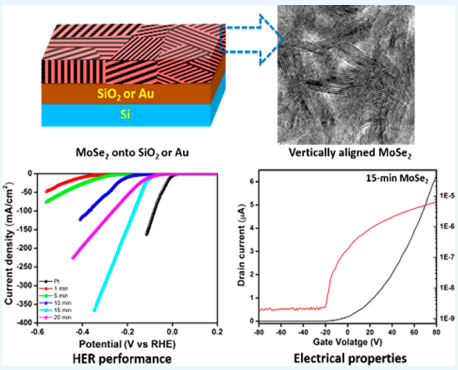

INTRODUCTION

As the interest in hydrogen (H_2) has continuously increased as a future sustainable energy source because of its high energy density without environmental pollution,[1,2] massive efforts have been devoted to develop efficient processes for H_2 production. One of the most effective and eco-friendly approaches to produce H_2 is hydrogen evolution reaction (HER) from electrochemical water splitting, which utilizes appropriate catalysts.[3,4] Platinum (Pt) and its alloys have been acknowledged as the most active catalyst for this reaction because they can dramatically improve the energy conversion efficiency by significantly dropping the overpotential to drive the reaction;[5,6] however, their scarcity and high cost hinder its large-scale use for H_2 production. In recent years, layered transition metal dichalcogenides (TMDCs) such as MoS_2 and $MoSe_2$ have received great attention by showing their potentials as efficient electrocatalysts for the HER,[7−41] and their cost-effectiveness, chemical stability, and profusion further support their extension to future earth-abundant noble-metal-free electrocatalysts.

Each charge-neutral layer of TMDCs, which consists of covalently bonded three atomic sheets (e.g., center Mo- and adjacent two S-sheets in MoS_2), is stacked together by weak out-of-plane van der Waals interactions to form bulk-state. Therefore, those layered materials have two types of surfaces, which are terrace sites on the basal planes and edge sites on the side surfaces, providing highly anisotropic property including hydrogen adsorption free energy on each surface, ΔG_H, for HER. From the theoretical studies, in the TMDCs with the conventional semiconducting 2H phase, the basal plane has been known to be electrochemically inert ($\Delta G_H \approx 2$ eV),[42,43] thus limiting the catalytic activity of bulk-state TMDC materials and having initiated various research efforts to maximally expose the catalytically active edge site by controlling their nanostructures to increase the edge to the basal plane ratio;[7−16,18] however, all those performances are still far behind of Pt-based catalysts. Alternatively, improving the catalytic activity of both basal and edge planes by transforming semiconducting 2H phase to 1T metallic phase (e.g., lithium intercalation) has been acknowledged to improve the HER performance of TMDCs,[16,17,25,31,39] but the process is cost-

Received: March 12, 2018
Accepted: May 16, 2018
Published: May 30, 2018

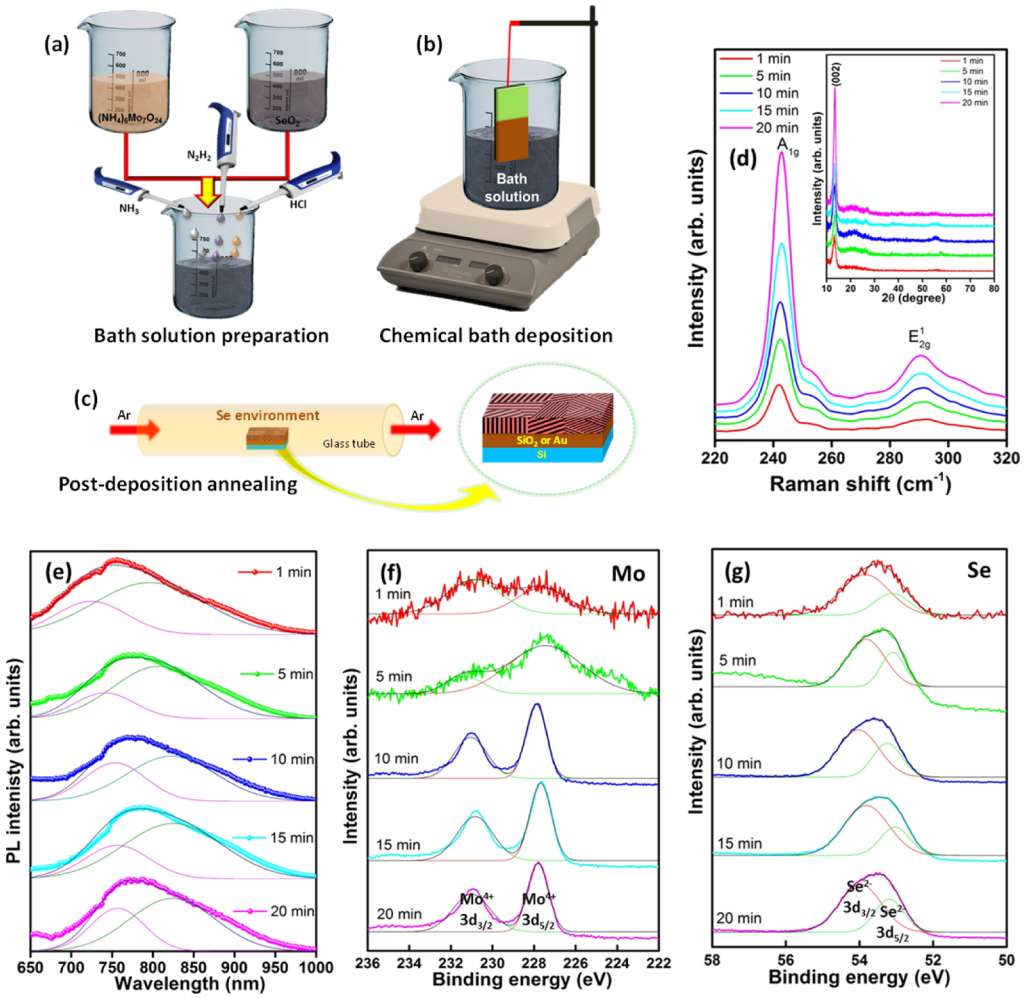

Figure 1. Characteristics of $MoSe_2$ thin films. (a–c) Schematic representation of (a) solution preparation, (b) thin film deposition of the CBD process for the vertically aligned layered $MoSe_2$ films, and (c) post-deposition annealing for the enhancement of the crystallinity of $MoSe_2$ thin films in a Se environment using a tubular furnace. (d) Raman spectra (inset: X-ray diffraction patterns). (e) PL with their deconvoluted spectra. (f,g) XPS signals with their deconvoluted spectra for (f) Mo and (g) Se.

ineffective as well as time-consuming, and the stability of metastable 1T phase would be an issue to be solved. In addition to increasing the number of active sites, enhancing the charge transport property of the TMDC-based catalyst could be another crucial factor to improve the HER performance, and therefore, approaches such as chemical doping of TMDCs to increase their inherent conductivity[20−22] and constructing hybrid nanostructures with highly conductive platforms[23−39] were demonstrated. However, the overall process could be complicated with the introduction of the additional materials, also inducing an increase in cost, compared to that of pristine TMDSs, and the grown TMDC layers, which were usually parallel to the substrate, had the inherently high resistance through the basal planes connected by van der Waals bond, inducing the limited performances.

In this work, a simple solution-based cost-effective methodology, which can grow $MoSe_2$ layers vertically aligned on substrates regardless of their types, maximizing the exposed active edge sites as well as charge transport property, is realized. $MoSe_2$ has known to have higher intrinsic conductivity with lower conduction band minimum[44] and better hydrogen adsorption coverage[36] than those of MoS_2. Consequently, it is proven that the catalytic performances of pristine $MoSe_2$ thin film having vertically aligned atomic layers could be significantly improved to produce outstanding HER catalytic performances with low overpotential of 88 mV at 10 $mA{\cdot}cm^{-2}$, an extremely high exchange current density of 0.845 $mA{\cdot}cm^{-2}$, and excellent stability, superior to most of the other reported MoS_2 or $MoSe_2$-based catalysts, even without additional strategies such as doping, phase transformation, and integration with other materials.

RESULTS AND DISCUSSION

Synthesis of $MoSe_2$ Thin Film Having Vertically Aligned Layered Structure. The synthesis of vertically aligned $MoSe_2$ layers was achieved on different substrates (SiO_2/Si and Au/Si) using a cost-effective chemical bath deposition (CBD) method.[45] Dissimilar to the traditional solution-based coating methods such as spin-coating, this approach can be utilized for various substrates regardless of the type, shape, and size. As shown in Figure 1a–c, the substrates were immersed in the precursor solution containing ammonium molybdate ($(NH_4)_6Mo_7O_{24}$) and selenium dioxide (SeO_2), and hydrazine hydrate (N_2H_4) and ammonia solution (NH_3) were involved in the reaction kinetics to form clear bath solution without any precipitation. Additionally, hydrochloric acid (HCl) was utilized to adjust the solution pH. The prepared

DOI: 10.1021/acsomega.8b00459
ACS Omega 2018, 3, 5799−5807

$MoSe_2$ thin films were post-annealed at 450 °C in a Se environment to improve the crystallinity of the $MoSe_2$ layers. The detailed experimental conditions are described in the Methods section. The overall reaction proceeded as follows (eq 1):

$$\frac{1}{7}(NH_2)_6Mo_7O_{24} + 2SeO_2 + \frac{1}{7}NH_3 + \frac{2}{7}N_2H_4 \rightarrow MoSe_2 + NH_4OH + \frac{2}{7}N_2\uparrow + 3\frac{3}{14}O_2\uparrow \quad (1)$$

In this process, the deposition time played a key role in the growth of $MoSe_2$, and it was changed from 1 to 20 min to adjust the thickness of the $MoSe_2$ thin film. The variation of surface morphology according to the deposition time was investigated by scanning electron microscopy (SEM) and atomic force microscopy (AFM), and transmission electron microscopy (TEM) was further utilized to unveil the structural information of the $MoSe_2$ layers within those thin films. SEM images in Figure 2a–e represent that smooth surface without any agglomerations was firstly formed (e.g., 1 and 5 min samples), and it evolved into uniformly distributed larger-sized spherical grains as the deposition time increased. This surface topology was further confirmed by AFM images (Figure 2k–o), and the thicknesses of $MoSe_2$ thin films were estimated to be approximately 1.8 (1 min), 8.4 (5 min), 16.5 (10 min), 25.7 (15 min), and 33.8 nm (20 min) (inset of Figure 2k–o). This morphological evolution suggests that the $MoSe_2$ film formation process follows homogeneous nucleation, producing larger agglomeration with the increase of the film thickness. The layered structure of $MoSe_2$, comprising the thin film, was further investigated by TEM, and densely packed stripes, representing vertically aligned $MoSe_2$ layers, were observed within the spherical grains of thin films as shown in Figure 2f–j. From the TEM images, we could also confirm that the deposition time shorter than 15 min was not enough to grow the film to be the thickness forming the multiple vertically aligned stripes. Moreover, the less discernible stripes in 20 min sample show that $MoSe_2$ layers grow randomly after the optimum deposition time (15 min), and it is expected that the property of the $MoSe_2$ film would become similar to that of bulk film as its thickness increases. The surface profile image, with their FFT patterns, is shown in Figure S1, and the spacing between the stripes is approximately 6.4–6.5 Å (Table S1), consistent with the interlayer spacing of $MoSe_2$.[8,13,29] Because most part of the thin film was terminated by the catalytically active edge sites of $MoSe_2$ layers (e.g., 15 min sample), we could expect efficient catalytic reactions from those thin films.

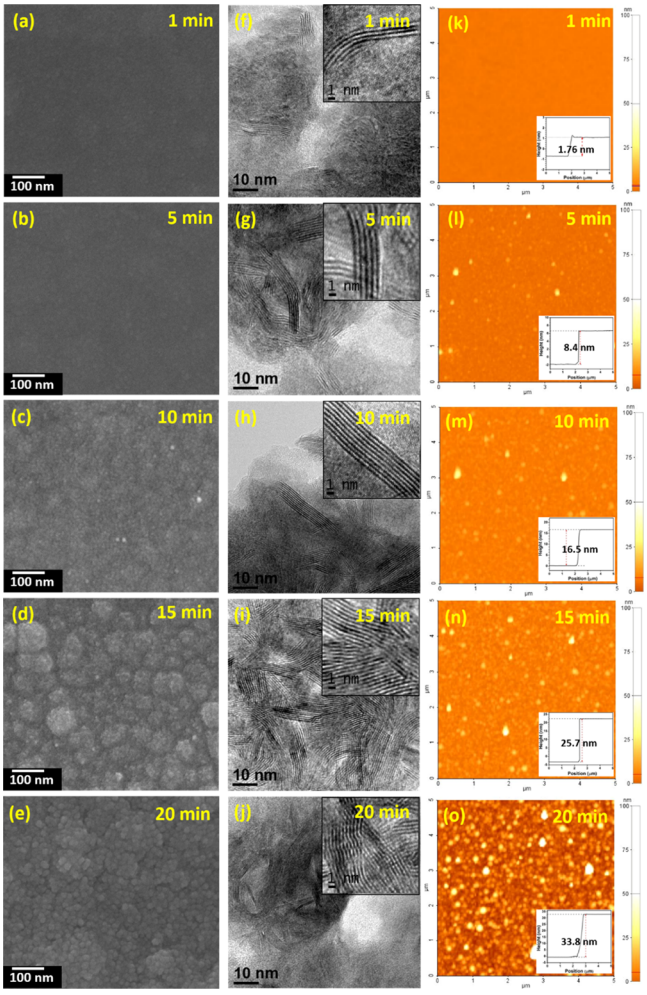

Figure 2. Nanomorphologies of $MoSe_2$ thin films. (a–e) SEM images, (f–j) TEM images (inset: high resolution), and (k–o) AFM topographical images (inset: AFM thickness profile spectra) of $MoSe_2$ thin films prepared with different deposition times, such as 1, 5, 10, 15, and 20 min.

Figure 1d shows the vibrational Raman modes of layered $MoSe_2$ thin films. The Raman profiles exhibited two characteristic phonon modes: one corresponded to the A_{1g} mode (242.01–242.89 cm^{-1}) associated with the out-of-plane vibration of Se atoms and the other corresponded to the E^1_{2g} mode (290.41–292.17 cm^{-1}) associated with the in-plane vibration of Mo and Se atoms.[46–48] Similar to the previous results in the literature,[47,48] A_{1g} and E^1_{2g} peaks exhibited blue and red shift, respectively, as the thickness increased with the deposition time. The wide range of Raman spectra in Figure S2 shows that the out-of-plane vibrational mode A_{1g} peaks are stronger than the characteristic peaks of the Si substrate (530 cm^{-1}), representing that the high-quality $MoSe_2$ layers are obtained using our CBD growth method.[47] Moreover, much higher A_{1g} peak about out-of-plane vibration than E^1_{2g} peak about in-plane vibration further supports our claim for the vertically aligned $MoSe_2$ layer structures,[13] consistent with the TEM results. The Raman mapping results with respect to the intensity of A_{1g} and E^1_{2g} mode peaks, obtained at 1 and 15 min-deposited samples over an area of 10 μm × 10 μm, are shown in Figure S3, which demonstrates uniform growth of $MoSe_2$. Additionally, the B^1_{2g} mode, which came from the broken translation symmetry along the c-axis direction, often found in few-layer samples, appeared at 352 cm^{-1} (Figure S2).[47,49,50] The crystal structure of $MoSe_2$ was also studied by X-ray diffraction (XRD) patterns as shown in the inset of Figure 1d, and (002) preferentially oriented peak was exhibited at 2θ = 13.45°, which is in agreement with the earlier report.[49] The (002) orientation lattice d-spacing values are estimated for different thickness $MoSe_2$ films, and they are compared with the TEM results as shown in Table S1.

The photoluminescence (PL) spectra of the $MoSe_2$ thin films obtained at the deposition times from 1 to 20 min are shown in Figure 1e. All spectra exhibit a broad peak, which can be deconvoluted to two separate peaks, and especially, those peaks in the thinnest film (1 min deposition), at 796 nm (1.56 eV) and 721 nm (1.72 eV), are similar to previous experimental results of A and B excitonic peaks observed in monolayer

DOI: 10.1021/acsomega.8b00459
ACS Omega 2018, 3, 5799–5807

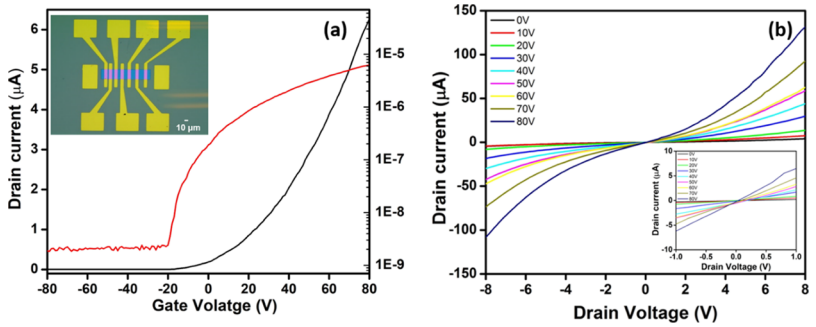

Figure 3. Electrical properties of 15 min-grown $MoSe_2$ thin film, characterized by FET. (a) Transfer characteristics (I_{DS} vs V_{GS}) of FET at V_{DS} = 1 V (inset: optical image of $MoSe_2$ FET). (b) Output characteristics (I_{DS} vs V_{DS}) of FET at various V_{GS} of 0−80 V (10 V step). The inset shows the I_{DS}−V_{DS} curves at low V_{DS} exhibiting a good linearity.

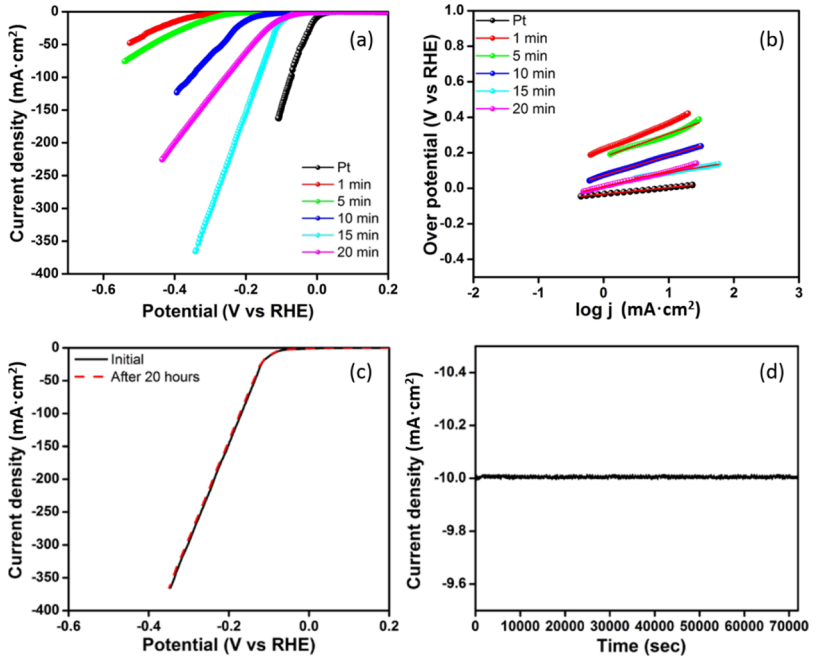

Figure 4. Electrocatalytic performances of $MoSe_2$ thin films. (a) Polarization curves. (b) Corresponding Tafel slopes. (c) Stability test for 20 h (15 min-grown sample). (d) Time course of the catalytic current during an electrolysis experiment (15 min-grown sample) at overpotential −88 mV vs RHE.

$MoSe_2$, respectively.[47,51] It has been known that those direct bandgaps of $MoSe_2$ are due to the quantum confinement effect in atomically thin $MoSe_2$ layers,[52] and large energy splitting of 0.1−0.4 eV in direct band transition peaks, originated from strong spin−orbit coupling, has been reported in monolayer TMDCs.[48,53,54] Meanwhile, X-ray photoelectron spectroscopy (XPS) analysis was performed to measure the binding energies of Mo and Se. For the 1 min deposited $MoSe_2$, Mo 3d peaks are observed at 230.9 and 227.7 eV (Figure 1f), which are ascribed to the doublet of Mo $3d_{3/2}$ and Mo $3d_{5/2}$, respectively.[55] Furthermore, Se 3d XPS deconvoluted spectra revealed that the Se $3d_{3/2}$ and $3d_{5/2}$ peaks were at 53.9 and 53.2 eV, respectively (Figure 1g). The detailed XPS peak positions and their intensities are provided in Table S2. Thicker films also have similar characteristics, and all the observed results are in highly consistent with the earlier reported values for $MoSe_2$.[47] The XPS survey spectra are shown in Figure S4.

Electrical Property of $MoSe_2$ Thin Films. In order to evaluate the electrical properties of the $MoSe_2$ thin films, bottom-gate field-effect transistors (FETs) were fabricated using those thin films grown on SiO_2/Si. Optical images of the prepared devices are shown in the insets of Figures 3a and S5. The field-effect mobility, μ_{FE}, was calculated from the slope of $\Delta I_{DS}/\Delta V_{GS}$ fitted to the linear regime of the transfer curves using the following equation (eq 2):

$$\mu_{FE} = \frac{L}{WC_{OX}V_{DS}}\frac{\Delta I_{DS}}{\Delta V_{GS}} \quad (2)$$

where W is the width of the channel (10 μm), L is the length of the channel (10 μm), C_{ox} is the capacitance per unit area of the gate dielectric (1.15×10^{-8} F·cm^{-2}), V_{DS} is the applied drain voltage (V_{DS} = 1 V), and $\Delta I_{DS}/\Delta V_{GS}$ is the slope in the linear part of the transfer plot (I_{DS}−V_{GS}) or transconductance (g_m). The g_m, μ_{FE}, and on/off current ratio were approximately 2.82×10^{-9} S, 0.24 cm^2·V^{-1}·s^{-1}, and 10^5, respectively, at V_{DS} = 1 V for the lowest-thickness $MoSe_2$ (1 min-grown) FET (Figure S5a). The values increased to approximately 1.01×10^{-7} S, 8.8 cm^2·V^{-1}·s^{-1}, and 10^5, respectively, at V_{DS} = 1 V for the higher-thickness $MoSe_2$ (15 min-grown) FET (Figure 3a,b). For the highest-thickness $MoSe_2$ (20 min-grown) FET (Figure S5b),

DOI: 10.1021/acsomega.8b00459
ACS Omega 2018, 3, 5799−5807

Table 1. Comparison of the Catalytic Performances of This Work with the Reported Values

	electrocatalyst	overpotential (mV)@ 10 mA·cm^{-2}	Tafel slope (mV·dec^{-1})	exchange current density (mA·cm^{-2})	refs
MoS_2 or $MoSe_2$	**vertically aligned $MoSe_2$ by CBD**	**88**	**59.8**	**0.845**	**this work**
	vertical arrays of stepped MoS_2	104	59	0.2	7
	network or flowerlike $MoSe_2$	228	92		8
	MoS_2 treated by O_2 plasma or annealed by H_2	>600	147−171	0.00038	9
	dendritic MoS_2	∼225	73	0.0245	10
	nanotriangular MoS_2	∼200	61	0.0381	11
	hierarchical $MoSe_{2-x}$ nanosheets	∼290	98		12
	vertically aligned $MoSe_2$	>450	105−120	0.002	13
	defect-rich MoS_2	∼190	50		14
	exfoliated MoS_2	∼210	70		15
	intercalation of vertically aligned $MoSe_2$ by Li^+	168	44	0.00025	16
	1T MoS_2 exfoliated by Li intercalant	∼200	40		17
	double-gyroid MoS_2	∼230	50	0.00069	18
MoS_2 or $MoSe_2$ + doping	Pt-doped MoS_2 nanosheets	∼140	96		20
	S-doped $MoSe_2$ nanosheets	∼100	60		21
	Ni-doped vertically aligned $MoSe_2$ on carbon fiber	250	59.8	0.00038	22
MoS_2 or $MoSe_2$-based hybrid	$MoSe_2$−RGO (with PVP) nanosheets	∼200	70		23
	MoS_2−CuS_x nanocomposite	100	39		24
	hydrazine-treated MoO_x−MoS_2 core−shell nanowires	>300	50	0.045	25
	$MoS_{2(1-x)}Se_{2x}$ particles on $NiSe_2$ form	69	42.1	0.2994	26
	NiSe nanocrystallites on $MoSe_2$ nanosheets	210	56		27
	$MoSe_2$ nanosheets decorated on carbon Fiber	182	69−76	0.0233	28
	$MoSe_2$ nanoflowers on RGO nanosheets	195	67		29
	MoS_2-coated $CoSe_2$ nanobelts	68	36	0.073	30
	Li-treated MoO_x−MoS_2 core−shell nanowires	∼290	52		31
	perpendicularly oriented $MoSe_2$ on SnO_2 nanotubes	174	51		32
	perpendicularly oriented $MoSe_2$ on graphene nanosheets	159	61		33
	MoS_2 nanosheets on SnO_2 nanotubes	∼220	59		34
	amorphous MoS_x on dealloyed nanoporous Au	∼220	41		35
	$MoSe_2$ nanosheets on RGO	115	69		36
	MoS_2 nanosheets between RGO sheets	∼170	41		37
	$MoS_{1.0}Se_{1.0}$ alloy	∼200	56	0.32	38
	Li-intercalated MoS_2 nanoparticles on the carbon fiber	>110	62	0.167	39

DOI: 10.1021/acsomega.8b00459
ACS Omega 2018, 3, 5799−5807

the g_m, μ_{FE}, and on/off current ratio decreased to approximately 6.86×10^{-9} S, 0.59 $cm^2 \cdot V^{-1} \cdot s^{-1}$, and 10^5, respectively, at V_{DS} = 1 V, and this may be due to the nature of the film becoming the bulk-state. The prepared $MoSe_2$ FETs showed a little lower performance than the chemical vapor deposition-grown $MoSe_2$ nanosheet-based devices because of the vertically aligned layered structure, and their electrical properties are expected to be further improved by applying the suitable processes such as post-annealing and doping.

Application of $MoSe_2$ Thin Films to HER. To validate the electrocatalytic behavior of the vertically aligned $MoSe_2$ for the HER, $MoSe_2$ was grown on an Au (200 nm)/Si substrate. Using the standard three-electrode system, the linear sweep voltammetry (LSV) polarization curves of the samples in a 0.5 M H_2SO_4 electrolyte solution were recorded with a scan rate of 2 $mV \cdot s^{-1}$. Figure 4a shows the LSV curves for the HER activity of the $MoSe_2$ thin films, grown for various deposition times. As a reference, a commercially available Pt electrode was compared. The lowest onset overpotential value at 10 $mA \cdot cm^{-2}$ ($\eta_{10mA \cdot cm^{-2}}$) is found from the 15 min-grown $MoSe_2$ to be −88 [mV vs reversible hydrogen electrode (RHE)], which is superior to most of the MoS_2 and $MoSe_2$-based HER catalysts,[7−41] including those with the dopant,[20−22] phase-transformed TMDCs,[16,17,25,31,39] and nanohybrid with other materials[23−39] (Table 1). This value increases with a decrease of deposition time because of insufficient thickness, and the observed onset overpotential values are at −367, −296, and −185 (mV vs RHE) for 1, 5, and 10 min-grown $MoSe_2$ films, respectively. It also increases slightly to −95 (mV vs RHE) for the 20 min-grown sample, and it is believed that the $MoSe_2$ film in this thickness range has more bulk nature, which has the reduced conductivity and the decreased number of active edge site, consequently degrading its electrocatalytic properties. Additionally, the maximum cathodic current density (j) value of 365 $mA \cdot cm^{-2}$ (at a overpotential of 341 mV) was estimated for 15 min-grown $MoSe_2$, which is superior to that of reference (Pt, 162 $mA \cdot cm^{-2}$ at a overpotential of 109 mV). The outstanding hydrogen evolution property of 15 min-grown $MoSe_2$ is revealed by the maximum "j" value, which is directly proportional to the amount of evolved hydrogen.[14]

The Tafel slope values were estimated from the Tafel plots (Figure 4b). The extracted lowest slope value was approximately 59.8 $mV \cdot dec^{-1}$ for the 15 min-deposited $MoSe_2$, suggesting excellent kinetic behavior, and the value increased with a decrease in deposition time (107 $mV \cdot dec^{-1}$ at 10 min, 125 $mV \cdot dec^{-1}$ at 5 min, and 150 $mV \cdot dec^{-1}$ at 1 min). Twenty minute-deposited sample also showed a slightly higher value, 87 $mV \cdot dec^{-1}$, than the 15 min-deposited sample. The Tafel slope is an intrinsic characteristic of the electrocatalyst and calculated by the rate-limiting step of the HER curves.[11] From the hydrogen evolution mechanism, this can be explained by the Volmer reaction, shown in eq 3, followed by the electrochemical desorption of H_{ads}, known as the Heyrovsky reaction, shown in eq 4. A recombination step, Tafel reaction, is also engaged in this process, as expressed in eq 5. The reactions are listed as follows:

$$H_3O^+ + e^- \rightarrow H_{ads} + H_2O \quad (3)$$

$$H_{ads} + H_3O^+ + e^- \rightarrow H_2 + H_2O \quad (4)$$

$$H_{ads} + H_{ads} \rightarrow H_2 \quad (5)$$

The exchange current density (j_0), a crucial parameter in the HER performance, was extracted for all the samples from the extrapolation of Tafel plots (Figure 4b). Particularly, the 15 min-grown $MoSe_2$ exhibits a remarkably high j_0 of 0.845 $mA \cdot cm^{-2}$, which is one of the maximum values among the reported MoS_2 and $MoSe_2$-based catalysts,[7−41] as presented in Table 1. In earlier reports, Cui et al.[13,22] have reported the vertically aligned $MoSe_2$ layers, but their performances were much lower than our results. The superior HER parameters from this work are summarized in Table S3.

To further investigate the interface reactions and electrode kinetics during the catalytic HER process, electrochemical impedance spectroscopy (EIS) was performed. From the Nyquist plots in Figure S6, the charge-transfer resistances (R_{CT}) of the $MoSe_2$ deposited for 20, 15, 10, 5, and 1 min were observed at 4.09, 3.61, 6.91, 8.61, and 13.74 Ω, respectively, and that of the Pt electrode was 20.83 Ω. The 15 and 20 min-grown $MoSe_2$ samples showed much lower R_{CT} values than those deposited for shorter times and Pt reference (the lowest value was shown from 15 min-grown $MoSe_2$), which was due to the more active site for H^+ reduction at the electrode−electrolyte interface. In addition, the small series resistances (R_s) of all the $MoSe_2$ samples (3.37 Ω: 20 min, 2.29 Ω: 15 min, 4.51 Ω: 10 min, 4.27 Ω: 5 min, and 3.06 Ω: 1 min), representing efficient electrical contact at the interface of the electrode with minimized parasitic Ohmic losses, are favorable for the practical applications.

Besides the HER activity, the stability is another important criterion to evaluate the electrocatalytic properties. To investigate the durability in an acidic environment, long-term cycling tests were conducted. Figure 4c shows that the performances of the 15 min deposited sample are not noticeably changed even after 20 h test, indicating its superior electrocatalytic stability for the long-term HER performance. Moreover, the time versus current density curve in Figure 4d shows the consistent current generation for the stable hydrogen molecule production over 20 h at a constant overpotential of −88 mV (15 min deposited $MoSe_2$).

CONCLUSIONS

In this work, vertically aligned $MoSe_2$ layers, maximizing the accessibility to the active edge sites and charge transport property simultaneously, were demonstrated by newly designed low-cost solution-based CBD process. The proposed preparation process is simple, scalable, and inexpensive, and the applicability to various substrates regardless of type and shape could offer a boundless opening to the preparation of layered structures. Even without additional strategies such as doping, phase transformation, and integration with other materials, the resultant pristine $MoSe_2$ films exhibited a low overpotential of 88 mV (at 10 $mA \cdot cm^{-2}$) and noticeably a high exchange current density of 0.845 $mA \cdot cm^{-2}$ with excellent stability, superior to most of the reported MoS_2 and $MoSe_2$-based electrocatalysts in the references. We believe that the methodology described in this work for superior HER performance with the long-term stability of $MoSe_2$ catalyst guides to the development of efficient practical hydrogen production catalysts.

METHODS

Synthesis of Vertically Aligned $MoSe_2$ Layers. The CBD process was utilized to synthesize $MoSe_2$ thin films. The

DOI: 10.1021/acsomega.8b00459
ACS Omega 2018, 3, 5799−5807

precursor solution bath was prepared by 0.03 M ammonium molybdate ($(NH_4)_6Mo_7O_{24}$) and 0.005 M selenium dioxide (SeO_2). The hydrazine hydrate (N_2H_4, 1.0 M) and ammonia solution (NH_3, 4 M) were added to form a clear bath solution without any precipitation. Hydrochloric acid (HCl) was used to control the solution pH (12 ± 0.1). The deposition time was varied to control the thickness of the $MoSe_2$ films (1, 5, 10, 15, and 20 min). SiO_2 (300 nm)/Si and Au (200 nm)/Si were utilized as substrates for FET and HER devices, respectively. The bath temperature was 90 °C. The prepared $MoSe_2$ layers were subjected to post-annealing treatment at 450 °C for 60 min in a Se atmosphere.

Characterization of $MoSe_2$ Films. The Renishaw inVia Raman microscope (model: RE04) was used to characterize $MoSe_2$ films with a scan speed of 30 s. XRD analysis was conducted with a Rigaku D/Max-2500 diffractometer, using a source of Cu Kα radiation. XPS analysis was performed using a PHI 5000 VersaProbe (25 W Al Kα, 6.7×10^{-8} Pa). The room temperature PL analysis was performed using a HORIBA microspectrometer with a spot size of 1 μm by the Nd:YAG laser source (532 nm wavelength). The surface morphology of $MoSe_2$ films was analyzed using field emission-SEM (JEOL JSM-6700F). Topology and film thickness were estimated using AFM (Vecco Dimension 3100). The vertically aligned $MoSe_2$-layered structures were confirmed with a support of a JEOL-2010F high-resolution transmission electron microscope. For TEM sample preparation, PMMA was coated onto the as-deposited $MoSe_2$ sample (on SiO_2/Si) and then SiO_2 was etched using KOH solution. After etching SiO_2, PMMA with $MoSe_2$ was floated on KOH solution, and it was transferred to the TEM Cu grid. The transferred sample was cleaned using acetone to remove poly(methyl methacrylate) (PMMA) for analysis. The FFT and R-FFT images were extracted using the Gatan DigitalMicrograph (version 3.21).

Electrochemical Measurements. LSV measurements were performed in the acidic electrolyte solution of 0.5 M H_2SO_4 (purged with pure N_2) with the scan rate of 2 mV·s^{-1}. The three-electrode system, which comprised a working electrode ($MoSe_2$-deposited Au), a counter electrode (graphite rod), and a reference electrode (saturated calomel electrode), was used for the LSV measurement. Au substrate was utilized to decrease the Ohmic resistance, and it was shown that the catalytic property of Au-only substrate was not noticeable.[11] The EIS measurements were performed with frequencies ranging from 10^5 to 0.1 Hz. The LSV curves were *iR*-corrected with the R_s values calculated from the EIS measurement.

Construction of the $MoSe_2$ FET Devices. The proposed CBD process was employed to prepare different thicknesses of $MoSe_2$ films onto SiO_2 (300 nm)/Si substrates for the FET device fabrication. The combination of photolithography and reactive ion SF_6/O_2 plasma etching was used to make the device structure and contact points. Ti/Au (10/50 nm) was deposited on $MoSe_2$ films onto SiO_2 (300 nm)/Si via electron beam evaporation as source/drain (S/D) electrode patterns. To remove the resist residue affecting the contact resistance, the prepared devices were annealed at 200 °C for 2 h in a tubular furnace with the 100 sccm Ar flow after preparing the electrode contacts. The fabricated $MoSe_2$ transistors were characterized using a two-probe technique at room temperature in a vacuum chamber to avoid oxidation.

■ ASSOCIATED CONTENT

Supporting Information

The Supporting Information is available free of charge on the ACS Publications website at DOI: 10.1021/acsomega.8b00459.

TEM characterization of 15 min-grown $MoSe_2$; the wide range of the Raman spectra of the $MoSe_2$ thin films; Raman mapping analysis; XPS survey scan for the $MoSe_2$ films grown for different deposition times; transfer characteristics of FETs (1 and 20 min-grown $MoSe_2$ thin film FETs); Nyquist plots of Pt and $MoSe_2$ thin-film-based samples; lattice spacing values of $MoSe_2$ from XRD and TEM; XPS peak positions and their intensity; and summary of the catalytic parameters in this work (PDF)

■ AUTHOR INFORMATION

Corresponding Author

*E-mail: huijoon@ajou.ac.kr (H.J.P.).

ORCID

Dhanasekaran Vikraman: 0000-0001-8991-3604
Seung-Hyun Chun: 0000-0001-8397-4481
Jongwan Jung: 0000-0002-1397-212X
Hyun-Seok Kim: 0000-0003-1127-5766
Hui Joon Park: 0000-0003-4607-207X

Notes

The authors declare no competing financial interest.

■ ACKNOWLEDGMENTS

This research was supported by MOTIE (10051565) and Korea Display Research Corporation (KDRC). This work was also supported by the Basic Science Research Program through the National Research Foundation of Korea (NRF), funded by the Ministry of Education (2010-0020207 and 2017R1D1A1B03034711).

■ REFERENCES

(1) Benck, J. D.; Hellstern, T. R.; Kibsgaard, J.; Chakthranont, P.; Jaramillo, T. F. Catalyzing the hydrogen evolution reaction (HER) with molybdenum sulfide nanomaterials. *ACS Catal.* **2014**, *4*, 3957−3971.

(2) Strmcnik, D.; Uchimura, M.; Wang, C.; Subbaraman, R.; Danilovic, N.; van der Vliet, D.; Paulikas, A. P.; Stamenkovic, V. R.; Markovic, N. M. Improving the hydrogen oxidation reaction rate by promotion of hydroxyl adsorption. *Nat. Chem.* **2013**, *5*, 300−306.

(3) Vesborg, P. C. K.; Seger, B.; Chorkendorff, I. Recent development in hydrogen evolution reaction catalysts and their practical implementation. *J. Phys. Chem. Lett.* **2015**, *6*, 951−957.

(4) Kibler, L. A. Hydrogen electrocatalysis. *ChemPhysChem* **2006**, *7*, 985−991.

(5) Greeley, J.; Stephens, I. E. L.; Bondarenko, A. S.; Johansson, T. P.; Hansen, H. A.; Jaramillo, T. F.; Rossmeisl, J.; Chorkendorff, I.; Nørskov, J. K. Alloys of platinum and early transition metals as oxygen reduction electrocatalysts. *Nat. Chem.* **2009**, *1*, 552−556.

(6) Greeley, J.; Jaramillo, T. F.; Bonde, J.; Chorkendorff, I.; Nørskov, J. K. Computational high-throughput screening of electrocatalytic materials for hydrogen evolution. *Nat. Mater.* **2006**, *5*, 909.

(7) Hu, J.; Huang, B.; Zhang, C.; Wang, Z.; An, Y.; Zhou, D.; Lin, H.; Leung, M. K. H.; Yang, S. Engineering stepped edge surface structures of MoS_2 sheet stacks to accelerate the hydrogen evolution reaction. *Energy Environ. Sci.* **2017**, *10*, 593−603.

(8) Guo, W.; Chen, Y.; Wang, L.; Xu, J.; Zeng, D.; Peng, D.-L. Colloidal synthesis of $MoSe_2$ nanonetworks and nanoflowers with

DOI: 10.1021/acsomega.8b00459
ACS Omega 2018, 3, 5799−5807

efficient electrocatalytic hydrogen-evolution activity. *Electrochim. Acta* **2017**, *231*, 69−76.
(9) Ye, G.; Gong, Y.; Lin, J.; Li, B.; He, Y.; Pantelides, S. T.; Zhou, W.; Vajtai, R.; Ajayan, P. M. Defects engineered monolayer MoS_2 for improved hydrogen evolution reaction. *Nano Lett.* **2016**, *16*, 1097−1103.
(10) Zhang, Y.; Ji, Q.; Han, G.-F.; Ju, J.; Shi, J.; Ma, D.; Sun, J.; Zhang, Y.; Li, M.; Lang, X.-Y.; Liu, Z. Dendritic, transferable, strictly monolayer MoS_2 flakes synthesized on $SrTiO_3$ single crystals for efficient electrocatalytic applications. *ACS Nano* **2014**, *8*, 8617−8624.
(11) Shi, J.; Ma, D.; Han, G.-F.; Zhang, Y.; Ji, Q.; Gao, T.; Sun, J.; Song, X.; Li, C.; Zhang, Y. Controllable growth and transfer of monolayer MoS_2 on Au foils and its potential application in hydrogen evolution reaction. *ACS Nano* **2014**, *8*, 10196−10204.
(12) Zhou, X.; Jiang, J.; Ding, T.; Zhang, J.; Pan, B.; Zuo, J.; Yang, Q. Fast colloidal synthesis of scalable Mo-rich hierarchical ultrathin $MoSe_{2-x}$ nanosheets for high-performance hydrogen evolution. *Nanoscale* **2014**, *6*, 11046−11051.
(13) Kong, D.; Wang, H.; Cha, J. J.; Pasta, M.; Koski, K. J.; Yao, J.; Cui, Y. Synthesis of MoS_2 and $MoSe_2$ films with vertically aligned layers. *Nano Lett.* **2013**, *13*, 1341−1347.
(14) Xie, J.; Zhang, H.; Li, S.; Wang, R.; Sun, X.; Zhou, M.; Zhou, J.; Lou, X. W. D.; Xie, Y. Defect-rich MoS_2 ultrathin nanosheets with additional active edge sites for enhanced electrocatalytic hydrogen evolution. *Adv. Mater.* **2013**, *25*, 5807−5813.
(15) Ji, S.; Yang, Z.; Zhang, C.; Liu, Z.; Tjiu, W. W.; Phang, I. Y.; Zhang, Z.; Pan, J.; Liu, T. Exfoliated MoS_2 nanosheets as efficient catalysts for electrochemical hydrogen evolution. *Electrochim. Acta* **2013**, *109*, 269−275.
(16) Wang, H.; Lu, Z.; Xu, S.; Kong, D.; Cha, J. J.; Zheng, G.; Hsu, P.-C.; Yan, K.; Bradshaw, D.; Prinz, F. B.; Cui, Y. Electrochemical tuning of vertically aligned MoS_2 nanofilms and its application in improving hydrogen evolution reaction. *Proc. Natl. Acad. Sci. U.S.A.* **2013**, *110*, 19701−19706.
(17) Voiry, D.; Salehi, M.; Silva, R.; Fujita, T.; Chen, M.; Asefa, T.; Shenoy, V. B.; Eda, G.; Chhowalla, M. Conducting MoS_2 nanosheets as catalysts for hydrogen evolution reaction. *Nano Lett.* **2013**, *13*, 6222−6227.
(18) Kibsgaard, J.; Chen, Z.; Reinecke, B. N.; Jaramillo, T. F. Engineering the surface structure of MoS_2 to preferentially expose active edge sites for electrocatalysis. *Nat. Mater.* **2012**, *11*, 963−969.
(19) Damien, D.; Anil, A.; Chatterjee, D.; Shaijumon, M. M. Direct deposition of $MoSe_2$ nanocrystals onto conducting substrates: towards ultra-efficient electrocatalysts for hydrogen evolution. *J. Mater. Chem. A* **2017**, *5*, 13364−13372.
(20) Deng, J.; Li, H.; Xiao, J.; Tu, Y.; Deng, D.; Yang, H.; Tian, H.; Li, J.; Ren, P.; Bao, X. Triggering the electrocatalytic hydrogen evolution activity of the inert two-dimensional MoS_2 surface via single-atom metal doping. *Energy Environ. Sci.* **2015**, *8*, 1594−1601.
(21) Xu, C.; Peng, S.; Tan, C.; Ang, H.; Tan, H.; Zhang, H.; Yan, Q. Ultrathin S-doped $MoSe_2$ nanosheets for efficient hydrogen evolution. *J. Mater. Chem. A* **2014**, *2*, 5597−5601.
(22) Wang, H.; Kong, D.; Johanes, P.; Cha, J. J.; Zheng, G.; Yan, K.; Liu, N.; Cui, Y. $MoSe_2$ and WSe_2 nanofilms with vertically aligned molecular layers on curved and rough surfaces. *Nano Lett.* **2013**, *13*, 3426−3433.
(23) Dai, C.; Zhou, Z.; Tian, C.; Li, Y.; Yang, C.; Gao, X.; Tian, X. Large-Scale Synthesis of Graphene-Like $MoSe_2$ Nanosheets for Efficient Hydrogen Evolution Reaction. *J. Phys. Chem. C* **2017**, *121*, 1974−1981.
(24) Bae, C.; Ho, T. A.; Kim, H.; Lee, S.; Lim, S.; Kim, M.; Yoo, H.; Montero-Moreno, J. M.; Park, J. H.; Shin, H. Bulk layered heterojunction as an efficient electrocatalyst for hydrogen evolution. *Sci. Adv.* **2017**, *3*, e1602215.
(25) Cummins, D. R.; Martinez, U.; Kappera, R.; Voiry, D.; Martinez-Garcia, A.; Jasinski, J.; Kelly, D.; Chhowalla, M.; Mohite, A. D.; Sunkara, M. K. Catalytic Activity in Lithium-Treated Core−Shell MoO_x/MoS_2 Nanowires. *J. Phys. Chem. C* **2015**, *119*, 22908−22914.
(26) Zhou, H.; Yu, F.; Huang, Y.; Sun, J.; Zhu, Z.; Nielsen, R. J.; He, R.; Bao, J.; Goddard, W. A., III; Chen, S.; Ren, Z. Efficient hydrogen evolution by ternary molybdenum sulfoselenide particles on self-standing porous nickel diselenide foam. *Nat. Commun.* **2016**, *7*, 12765.
(27) Zhou, X.; Liu, Y.; Ju, H.; Pan, B.; Zhu, J.; Ding, T.; Wang, C.; Yang, Q. Design and epitaxial growth of $MoSe_2$−NiSe vertical heteronanostructures with electronic modulation for enhanced hydrogen evolution reaction. *Chem. Mater.* **2016**, *28*, 1838−1846.
(28) Qu, B.; Yu, X.; Chen, Y.; Zhu, C.; Li, C.; Yin, Z.; Zhang, X. Ultrathin $MoSe_2$ Nanosheets Decorated on Carbon Fiber Cloth as Binder-Free and High-Performance Electrocatalyst for Hydrogen Evolution. *ACS Appl. Mater. Interfaces* **2015**, *7*, 14170−14175.
(29) Liu, Z.; Li, N.; Zhao, H.; Du, Y. Colloidally synthesized $MoSe_2$/graphene hybrid nanostructures as efficient electrocatalysts for hydrogen evolution. *J. Mater. Chem. A* **2015**, *3*, 19706−19710.
(30) Gao, M.-R.; Liang, J.-X.; Zheng, Y.-R.; Xu, Y.-F.; Jiang, J.; Gao, Q.; Li, J.; Yu, S.-H. An efficient molybdenum disulfide/cobalt diselenide hybrid catalyst for electrochemical hydrogen generation. *Nat. Commun.* **2015**, *6*, 5982.
(31) Cummins, D. R.; Martinez, U.; Sherehiy, A.; Kappera, R.; Martinez-Garcia, A.; Schulze, R. K.; Jasinski, J.; Zhang, J.; Gupta, R. K.; Lou, J.; Chhowalla, M.; Sumanasekera, G.; Mohite, A. D.; Sunkara, M. K.; Gupta, G. Efficient hydrogen evolution in transition metal dichalcogenides via a simple one-step hydrazine reaction. *Nat. Commun.* **2016**, *7*, 11857.
(32) Huang, Y.; Miao, Y.-E.; Fu, J.; Mo, S.; Wei, C.; Liu, T. Perpendicularly oriented few-layer $MoSe_2$ on SnO_2 nanotubes for efficient hydrogen evolution reaction. *J. Mater. Chem. A* **2015**, *3*, 16263−16271.
(33) Mao, S.; Wen, Z.; Ci, S.; Guo, X.; Ostrikov, K. K.; Chen, J. Perpendicularly oriented $MoSe_2$/graphene nanosheets as advanced electrocatalysts for hydrogen evolution. *Small* **2015**, *11*, 414−419.
(34) Huang, Y.; Miao, Y.-E.; Zhang, L.; Tjiu, W. W.; Pan, J.; Liu, T. Synthesis of few-layered MoS_2 nanosheet-coated electrospun SnO_2 nanotube heterostructures for enhanced hydrogen evolution reaction. *Nanoscale* **2014**, *6*, 10673−10679.
(35) Ge, X.; Chen, L.; Zhang, L.; Wen, Y.; Hirata, A.; Chen, M. Nanoporous Metal Enhanced Catalytic Activities of Amorphous Molybdenum Sulfide for High-Efficiency Hydrogen Production. *Adv. Mater.* **2014**, *26*, 3100−3104.
(36) Tang, H.; Dou, K.; Kaun, C.-C.; Kuang, Q.; Yang, S. $MoSe_2$ nanosheets and their graphene hybrids: synthesis, characterization and hydrogen evolution reaction studies. *J. Mater. Chem. A* **2014**, *2*, 360−364.
(37) Zheng, X.; Xu, J.; Yan, K.; Wang, H.; Wang, Z.; Yang, S. Space-confined growth of MoS_2 nanosheets within graphite: the layered hybrid of MoS_2 and graphene as an active catalyst for hydrogen evolution reaction. *Chem. Mater.* **2014**, *26*, 2344−2353.
(38) Kiran, V.; Mukherjee, D.; Jenjeti, R. N.; Sampath, S. Active guests in the $MoS_2/MoSe_2$ host lattice: efficient hydrogen evolution using few-layer alloys of MoS2(1−x) Se2x. *Nanoscale* **2014**, *6*, 12856−12863.
(39) Wang, H.; Lu, Z.; Kong, D.; Sun, J.; Hymel, T. M.; Cui, Y. Electrochemical tuning of MoS_2 nanoparticles on three-dimensional substrate for efficient hydrogen evolution. *ACS Nano* **2014**, *8*, 4940−4947.
(40) Xue, N.; Diao, P. Composite of Few-Layered MoS_2 Grown on Carbon Black: Tuning the Ratio of Terminal to Total Sulfur in MoS_2 for Hydrogen Evolution Reaction. *J. Phys. Chem. C* **2017**, *121*, 14413−14425.
(41) Xue, N.; Diao, P. Molybdenum Diselenide Nanolayers Prepared on Carbon Black as an Efficient and Stable Electrocatalyst for Hydrogen Evolution Reaction. *J. Phys. Chem. C* **2017**, *121*, 26686−26697.
(42) Hinnemann, B.; Moses, P. G.; Bonde, J.; Jørgensen, K. P.; Nielsen, J. H.; Horch, S.; Chorkendorff, I.; Nørskov, J. K. Biomimetic hydrogen evolution: MoS_2 nanoparticles as catalyst for hydrogen evolution. *J. Am. Chem. Soc.* **2005**, *127*, 5308−5309.

DOI: 10.1021/acsomega.8b00459
ACS Omega 2018, 3, 5799−5807

(43) Raybaud, P.; Hafner, J.; Kresse, G.; Kasztelan, S.; Toulhoat, H. Ab initio study of the H_2−H_2S/MoS_2 gas−solid interface: The nature of the catalytically active sites. *J. Catal.* **2000**, *189*, 129−146.
(44) Gupta, U.; Naidu, B. S.; Maitra, U.; Singh, A.; Shirodkar, S. N.; Waghmare, U. V.; Rao, C. N. R. Characterization of few-layer 1T-$MoSe_2$ and its superior performance in the visible-light induced hydrogen evolution reaction. *APL Mater.* **2014**, *2*, 092802.
(45) Vikraman, D.; Akbar, K.; Hussain, S.; Yoo, G.; Jang, J.-Y.; Chun, S.-H.; Jung, J.; Park, H. J. Direct synthesis of thickness-tunable MoS_2 quantum dot thin layers: Optical, structural and electrical properties and their application to hydrogen evolution. *Nano Energy* **2017**, *35*, 101−114.
(46) Wang, X.; Gong, Y.; Shi, G.; Chow, W. L.; Keyshar, K.; Ye, G.; Vajtai, R.; Lou, J.; Liu, Z.; Ringe, E.; Tay, B. K.; Ajayan, P. M. Chemical Vapor Deposition Growth of Crystalline Monolayer $MoSe_2$. *ACS Nano* **2014**, *8*, 5125−5131.
(47) Lu, X.; Utama, M. I. B.; Lin, J.; Gong, X.; Zhang, J.; Zhao, Y.; Pantelides, S. T.; Wang, J.; Dong, Z.; Liu, Z.; Zhou, W.; Xiong, Q. Large-Area Synthesis of Monolayer and Few-Layer $MoSe_2$ Films on SiO_2 Substrates. *Nano Lett.* **2014**, *14*, 2419−2425.
(48) Tonndorf, P.; Schmidt, R.; Böttger, P.; Zhang, X.; Börner, J.; Liebig, A.; Albrecht, M.; Kloc, C.; Gordan, O.; Zahn, D. R. T. Photoluminescence emission and Raman response of monolayer MoS_2, $MoSe_2$, and WSe_2. *Opt. Express* **2013**, *21*, 4908−4916.
(49) Jung, C.; Kim, S. M.; Moon, H.; Han, G.; Kwon, J.; Hong, Y. K.; Omkaram, I.; Yoon, Y.; Kim, S.; Park, J. Highly Crystalline CVD-grown Multilayer $MoSe_2$ Thin Film Transistor for Fast Photodetector. *Sci. Rep.* **2015**, *5*, 15313.
(50) Luo, X.; Zhao, Y.; Zhang, J.; Toh, M.; Kloc, C.; Xiong, Q.; Quek, S. Y. Effects of lower symmetry and dimensionality on Raman spectra in two-dimensional WSe_2. *Phys. Rev. B: Condens. Matter Mater. Phys.* **2013**, *88*, 195313.
(51) Shim, G. W.; Yoo, K.; Seo, S.-B.; Shin, J.; Jung, D. Y.; Kang, I.-S.; Ahn, C. W.; Cho, B. J.; Choi, S.-Y. Large-area single-layer $MoSe_2$ and its van der Waals heterostructures. *ACS Nano* **2014**, *8*, 6655−6662.
(52) Mak, K. F.; Lee, C.; Hone, J.; Shan, J.; Heinz, T. F. Atomically thin MoS_2: a new direct-gap semiconductor. *Phys. Rev. Lett.* **2010**, *105*, 136805.
(53) Beal, A. R.; Hughes, H. P. Kramers-Kronig analysis of the reflectivity spectra of 2H-MoS_2, 2H-$MoSe_2$ and 2H-$MoTe_2$. *J. Phys. C* **1979**, *12*, 881.
(54) Zhu, Z. Y.; Cheng, Y. C.; Schwingenschlögl, U. Giant spin-orbit-induced spin splitting in two-dimensional transition-metal dichalcogenide semiconductors. *Phys. Rev. B: Condens. Matter Mater. Phys.* **2011**, *84*, 153402.
(55) Song, I.; Park, C.; Hong, M.; Baik, J.; Shin, H.-J.; Choi, H. C. Patternable large-scale molybdenum disulfide atomic layers grown by gold-assisted chemical vapor deposition. *Angew. Chem., Int. Ed.* **2014**, *53*, 1266−1269.

DOI: 10.1021/acsomega.8b00459
ACS Omega 2018, 3, 5799−5807